

Origin of protons and light nuclei below the geomagnetic cutoff

L. Derome and M. Buénerd

Institut des Sciences Nucléaires, IN2P3, 53 av. des Martyrs, 38026 Grenoble cedex, France

Abstract. The flux of proton and light nuclei observed by AMS below the geomagnetic cutoff is accounted for by a simulation incorporating cosmic ray flux, magnetosphere, atmosphere, nucleon production cross section and coalescence model. Results of simulations for ${}^{1,2,3}H$ and ${}^{3,4}He$ are presented and compared to the data.

1 Introduction

Particles at high momenta have been observed recently in orbit close to earth by the first flight of the AMS experiment, providing new accurate measurements of Cosmic Ray (CR) flux. Large values of flux have been measured for protons (J. Alcaraz et al., 2000a) together while small but significant populations of helium and deuterium particles (J. Alcaraz et al., 2000c; G. Lamanna, 2000) below the geomagnetic cutoff (GC), with kinetic energies extending beyond 1 GeV per nucleon. The possible origins of these flux are discussed in this contribution on the basis of a Monte-Carlo simulation.

The observed intensity of the subGC proton flux in the equatorial region is about equal to the cosmic flux component above GC. It is maximum at low momenta and extends from the momentum threshold of the spectrometer at ≈ 0.4 GeV/c, up to GC around 10 GeV/c in the equatorial region, where the high momentum tail merges with the primary proton spectrum above GC. For light nuclei, the pattern for the $Z=2$ particle spectra observed above and below GC is highly peculiar since only 4He are observed above GC whereas only 3He are found below GC, with however a small admixture of the other isotope being compatible with the data in both cases (J. Alcaraz et al., 2000c). This pattern, together with the relative population of light nuclei, provide clues to the dynamical origin of the SubGC particles. It has been known for long that SubGC particles are secondaries produced by nuclear reaction between incoming cosmic ray (mainly proton and Helium) and atmospheric nuclei (mainly ${}^{14}N$ and ${}^{16}O$).

Correspondence to: M. Buénerd (derome@isn.in2p3.fr)

2 Simulation calculations

The inclusive particle spectra at the altitude of AMS have been calculated by means of a dedicated computer simulation program (see L. Derome et al. (2000); L. Derome and M. Buénerd (2001a) for details). The primary proton and helium flux used as input in this simulation are those measured by AMS (J. Alcaraz et al., 2000b,c). Particles are generated isotropically on a sphere at 500 km altitude. To take into account the geomagnetic cutoff, each generated particle is backtraced and only those reaching the outer space are then propagated. Propagation includes a detailed treatment of the geomagnetic field (N.A. Tsyganenko, 1995).

Particles can interact with atmospheric nuclei to produce secondary nucleons p , n , ${}^{2,3}H$ and ${}^{3,4}He$ with cross sections and multiplicities as discussed below. Each secondary particle is then propagated and allowed to interact as in the previous step. A reaction cascade can thus develop through the atmosphere. The reaction products are counted when they cross the virtual sphere at the altitude of the AMS spectrometer (380 km), upward and downward. All charged particles undergo energy loss by ionisation. Each event is propagated until the particle disappears by nuclear collision, stops in the atmosphere by energy loss, or escapes to outer space.

The proton induced proton production is generated as described in L. Derome and M. Buénerd (2001a) using the parametrization from A.N. Kalinovski et al. (1989). For incident 4He particles, the same spectral shape as for protons is used, appropriately scaled to account for the experimental 4He -nucleus total reaction cross section (J. Jaros et al., 1978) and proton production cross section (multiplicity) for 4He collisions on nuclei (D. Armutliiski et al., 1987; S. Baskovic et al., 1993).

The light nuclei production has also been implemented in the simulation program. Here, light nuclei can be produced either by the projectile fragmentation (only for 4He induced reaction) or by nucleon coalescence. In the latter model, nucleons coalesce when they fall within the coalescence radius in the final state of the collision (see L. Derome and

M. Buénerd (2001b) and the references inside for details).

2.1 Fragmentation model

For the ${}^4\text{He}$ fragmentation cross section, the model from A.S. Goldhaber (1974) was used. In this model, the fragment production cross section is proportional to $e^{-\frac{P^2}{\sigma^2}}$ in the projectile reference frame, with

$$\sigma^2 = \sigma_0^2 \frac{A_f(A_p - A_f)}{A_p - 1},$$

and P , A_p , A_f being the fragment momentum in this frame, projectile mass number, and fragment mass, respectively. The value of the Fermi momentum related parameter $\sigma_0=100$ MeV/c was from A.S. Goldhaber (1974); J. Mougey et al. (1981). The ${}^4\text{He}$ fragmentation production cross-sections for D , ${}^3\text{H}$ and ${}^3\text{He}$ particles, were from A.Kh. Abdurakhimov et al. (1981) and corrected for their $A^{1/3}$ dependence.

2.2 Coalescence model

In the coalescence model, the invariant differential production cross sections for composite fragments with mass A , can be related to the nucleon production cross section by a simple power law:

$$E_A \frac{d^3 N_A}{d\mathbf{p}_A^3} = B_A \left(E_p \frac{d^3 N_p}{d\mathbf{p}_p^3} \right)^A,$$

where $\mathbf{p}_A = A\mathbf{p}_p$. This relation provides straightforwardly the momentum spectrum of mass A fragments as a function of the nucleon spectrum. The input for the event cross section calculation then consist only of the proton production differential cross-section presented above and of the value of the B_A parameter. These parameters for p induced collisions have approximately constant values through the energy range from 0.2 GeV/n up to 70 GeV/n (J. Simon-Gillo et al., 1995). The following values, averaged from S. Nagamiya et al. (1981); G. Montarou et al. (1991); G.A. Safronov et al. (1988); N. Saito et al. (1994); V.V. Abramov et al. (1987), were used in the program: $B_2 = 2.5 \cdot 10^{-2}$ for deuteron, $B_3 = 2.5 \cdot 10^{-4}$ for ${}^3\text{He}$, $B'_3 = 4 \cdot 10^{-4}$ for ${}^3\text{H}$, and $B_4 = 4 \cdot 10^{-6}$ for ${}^4\text{He}$, in units $(\text{GeV}^2/c^3)^{(A-1)}$. The accuracy on these values is estimated to be within $\pm 30\%$ for B_2 , and $\pm 50\%$ for B_3 , B'_3 and B_4 .

3 Simulation results

The simulation has been run for $2 \cdot 10^8$ incident primary proton and helium particles generated at the injection sphere. This number corresponds to a sampling time of $4 \cdot 10^{-12}$ s of the cosmic ray flux. The results are shown on figures 1 to 4. Note that no adjustable parameter was involved in the calculations. An angular acceptance of 30 degrees with respect to the zenith has been assumed for the detector.

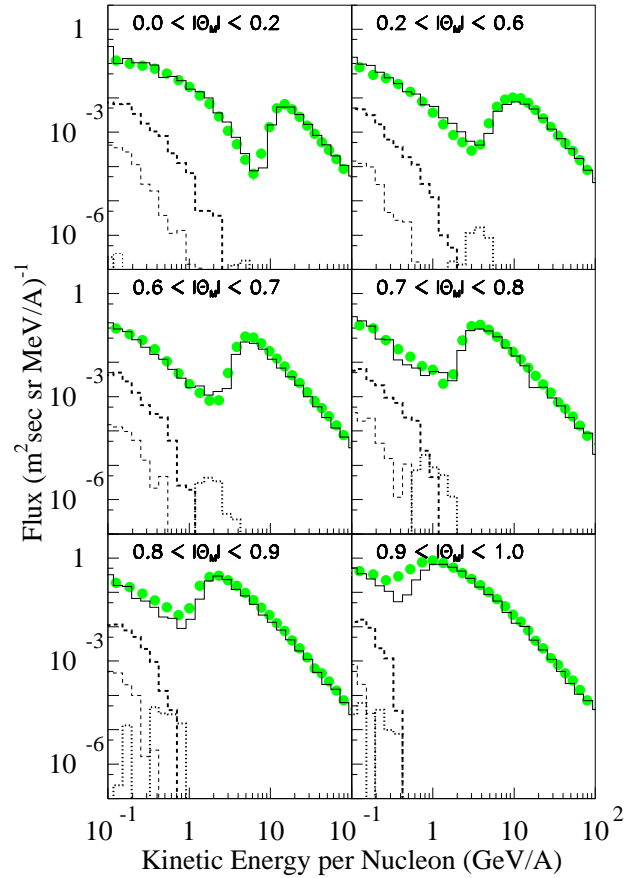


Fig. 1. Simulated spectra for downward p (primary+secondary) (solid lines), D from fragmentation (dotted lines), coalescence D (dashed thick lines), ${}^3\text{H}$ from coalescence (dashed thin lines) separate according to the CGM latitudes (θ_M). Full circles correspond to the experimental p spectra measured by AMS (J. Alcaraz et al., 2000a).

3.1 $Z=1$ spectra

Figure 1 shows the simulated spectra for $Z = 1$ particles compared with the experimental spectra measured by AMS (J. Alcaraz et al., 2000a) for 6 bins of corrected geomagnetic (CGM) latitude (A. Brekke, 1997). The agreement between the data and the simulation results is remarkably good, at all latitudes, both for primary and secondary (SubGC) p . In particular, the cutoff region is particularly well reproduced, which indicates that the processing of the particle dynamics and kinematics is good.

The expected spectra for $Z=1$ light nuclei are also shown on figure 1. For D , the contribution from ${}^4\text{He}$ fragmentation and coalescence are shown separately. The fragmentation yield is seen to be predicted mainly near the cutoff energy. This is due to the basic velocity-conserving property of the fragmentation process. Note that fragmentation and coalescence D yields merge at high latitudes. For ${}^3\text{H}$, this latter

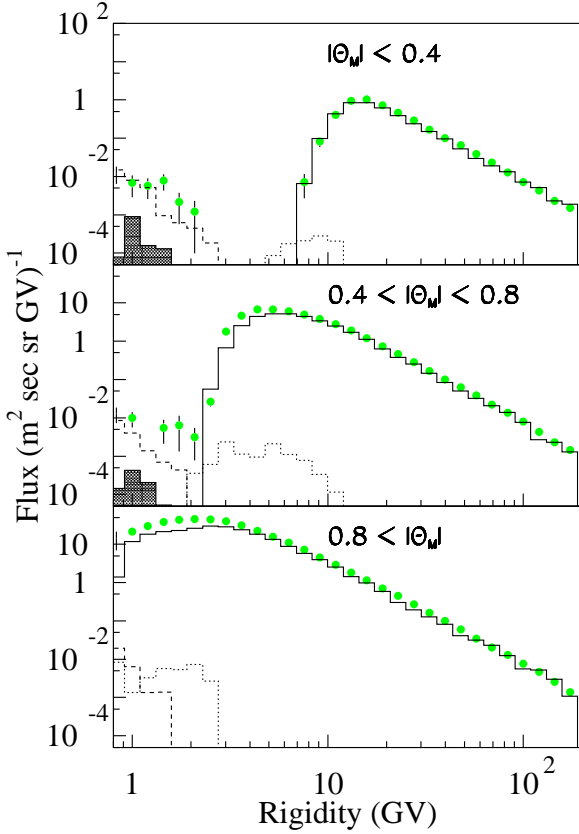


Fig. 2. Simulated Flux spectra for downward $Z = 2$ particles separate according to the CGM latitudes. The contribution of primary ${}^4\text{He}$ (solid lines), ${}^3\text{He}$ from fragmentation (dotted lines), coalescence ${}^3\text{He}$ (dashed lines) and coalescence ${}^4\text{He}$ (shaded histograms) are shown. Full circles correspond to the experimental $Z = 2$ particles flux spectra measured by AMS (J. Alcaraz et al., 2000c).

property gives the fragment a high rigidity value, larger than the cutoff rigidity. This explains the quasi-absence of downward fragmentation ${}^3\text{H}$. The SubGC flux are dominated by coalescence products and the large $D/{}^3\text{H}$ abundance ratio is a natural consequence of the coalescence model, the production cross-section decreasing with the increasing fragment mass number (larger probability for smaller cluster mass).

3.2 $Z = 2$ spectra

Figure 2 shows the comparison between the He spectra measured by AMS (full circle) (J. Alcaraz et al., 2000c) and the simulation results for 3 bins of CGM latitude. The solid histograms correspond to the ${}^4\text{He}$ cosmic ray flux above GC. It is seen that they reproduce fairly well the experimental distributions, with however a tendency to underestimate the experimental CR flux close to GC. The dotted histograms correspond to ${}^3\text{He}$ particles produced by ${}^4\text{He}$ fragmentation. As it was observed for fragmentation D yield, the expected flux is seen to be significant only close to GC, with the differential flux more than two order of magnitude smaller than the primary ${}^4\text{He}$ flux, except very close to cutoff. This value of

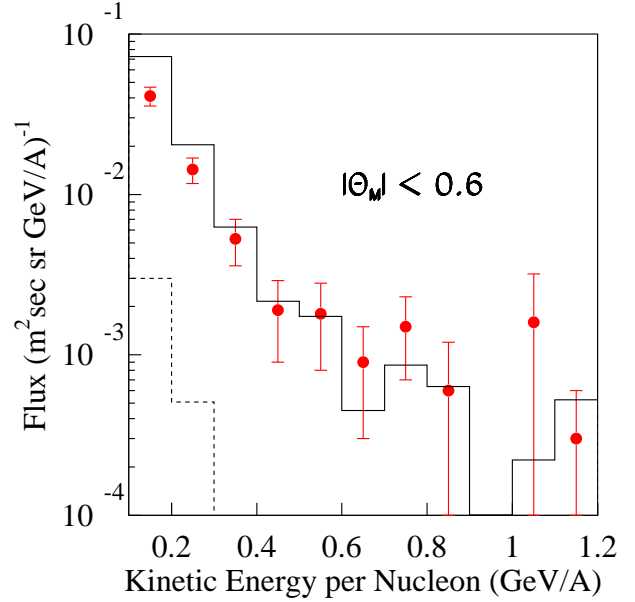


Fig. 3. Simulated Flux spectra for downward SubGC ${}^3\text{He}$ integrated over $|\theta_M| < 0.6$ rad compared with the ${}^3\text{He}$ flux spectra (full circle) measured by AMS (J. Alcaraz et al., 2000c). The dashed line corresponds to simulated the SubGC ${}^4\text{He}$ flux.

the fragmentation ${}^3\text{He}$ flux is small compared to the experimental CR ${}^3\text{He}$ flux (O. Reimer et al., 1998) which is about 10% of the CR ${}^4\text{He}$ flux for this momentum range, i.e. about ten times larger than the value calculated here. This result is compatible with the AMS measurements (see figure 4 in J. Alcaraz et al. (2000c)). The dashed and gray-shaded histograms correspond to CR p plus ${}^4\text{He}$ induced coalescence ${}^3\text{He}$ and ${}^4\text{He}$ flux respectively. The simulated ${}^3\text{He}$ spectra account pretty well for the measured SubGC $Z=2$ particle spectra both in magnitude and in shape.

Figure 3 shows the ${}^3\text{He}$ particle spectrum measured by AMS, in kinetic energy per nucleon, integrated over the latitude range $|\theta_M| < 0.6$ rad, compared to the simulation results. The calculated values are seen to be in good agreement with the data. The small ${}^4\text{He}$ coalescence yield (dashed line) is predicted to be more than one order of magnitude smaller, a value compatible with the AMS conclusions in which an experimental upper limit of 10% for this ratio was set.

3.3 Energy-integrated flux below GC

Figure 4 shows the energy integrated subGC AMS spectra for protons (J. Alcaraz et al., 2000a), ${}^3\text{He}$, and upper limit of ${}^4\text{He}$ (taken as 10% of the ${}^3\text{He}$ flux) (J. Alcaraz et al., 2000c), compared with simulation results. As mentioned above, the SubGC flux for light nuclei are dominated by the coalescence production. The hierarchy of flux magnitudes observed on figure 4 originates from the hierarchy of production yields, decreasing with the increasing mass number of the produced nucleus in the coalescence model.

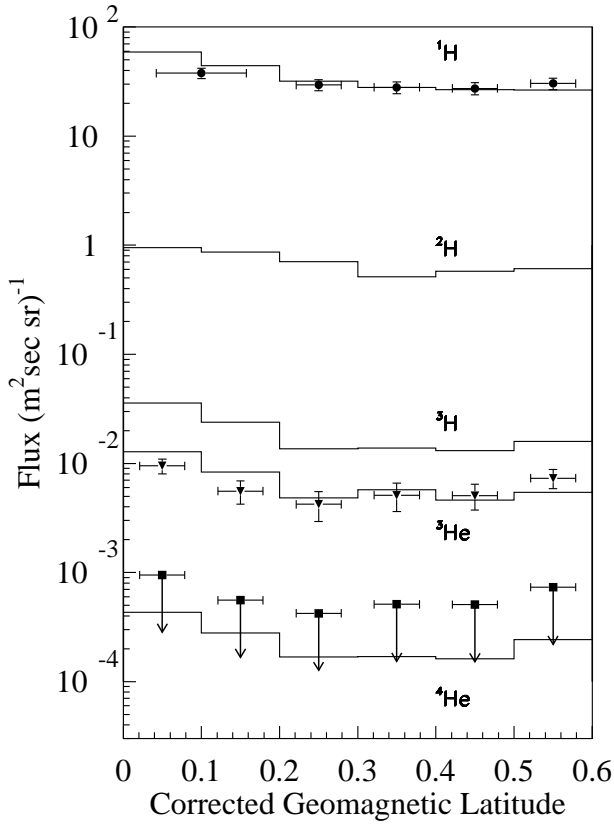


Fig. 4. Simulated SubGC flux as a function of the CGM latitude for the particle under consideration in this paper (solid lines). The SubGC p flux measured by AMS (full circle) have been obtained by integrating the SubGC part of the flux spectra given in J. Alcaraz et al. (2000a). The SubGC ${}^3\text{He}$ flux measured by AMS is shown (triangle) together with the upper limits for the SubGC ${}^4\text{He}$ flux (square) taken as 10 % of the SubGC ${}^3\text{He}$ flux (J. Alcaraz et al., 2000c).

4 Conclusion

It has been shown that the AMS measurements of proton and light nuclei flux can be reproduced consistently and simultaneously by a simulation incorporating the interactions between Cosmic Ray flux, earth magnetosphere and atmosphere, and assuming a composite fragment production by coalescence of nucleons induced by proton and ${}^4\text{He}$ collisions with atmospheric nuclei.

References

- A.Kh. Abdurakhimov et al., Nucl. Phys. A 362, 376, 1981.
 V.V. Abramov et al., Sov. J. of Nucl. Phys. 45, 845, 1987.
 J. Alcaraz et al., Phys. Lett. B 472, 215, 2000a.
 J. Alcaraz et al., Phys. Lett. B 490, 27, 2000b.
 J. Alcaraz et al., Phys. Lett. B 494, 19, 2000c.
 D. Armutliiski et al., Sov. J. of Nucl. Phys. 45, 649, 1987.
 S. Baskovic et al., Phys. At. Nucl. 56, 540, 1993.
 A. Brekke, Physics of the Upper Polar Atmosphere, Wiley, 1997.
 L. Derome et al., Phys. Lett. B 489, 1, 2000.
 L. Derome and M. Buénerd, Nucl. Phys. A 688, 66, 2001a.
 L. Derome and M. Buénerd, astro-ph/0105523, May 31, 2001b.
 A.S. Goldhaber, Phys. Lett. B 53, 306, 1974.
 J. Jaros et al., Phys. Rev. C 18, 2273, 1985.
 A.N. Kalinovski, M.V. Mokhov, and Yu.P. Nikitin, Passage of high energy particles through matter, AIP ed., 1989
 G. Lamanna, Thesis, University of Perugia, 2000.
 J. Mougey et al., Phys. Lett. B 105, 25, 1981.
 G. Montarou et al., Phys. Rev. C 44, 365, 1991.
 S. Nagamiya et al., Phys. Rev. C 24, 971, 1981.
 O. Reimer et al., ApJ. 496, 490, 1998.
 G.A. Safronov et al., Sov. J. of Nucl. Phys. 47, 966, 1988.
 N. Saito et al., Phys. Rev. C 49, 3211, 1994.
 J. Simon-Gillo et al., Nucl. Phys. A 590, 477c, 1995.
 C. Störmer, The Polar Aurora, Clarendon Press (Cambridge), 1955.
 N.A. Tsyganenko, J. Geophys. Res. 100, 5599, 1995.
 M.S. Vallarta, Handbuch der Physik, Springer Verlag, Vol 61/1, p 88, 1961.